Authors' Accepted Manuscript
Published in *ASCE-ASME Journal of Risk and Uncertainty in Engineering Systems, Part A: Civil Engineering*
https://doi.org/10.1061/AJRUA6.RUENG-1000

Shear Performance of Large-Thickness Precast Shear Walls with Cast-in-Place Belts and Grouting Sleeves

Linzi Fan[1]; Jialong Wei[2]; Yao Chen, Ph.D., M.ASCE[3];
Jian Feng, Ph.D.[4]; and Pooya Sareh, Ph.D.[5]

Abstract: Building industrialization has great significance for improving the efficiency of construction production, achieving the goal of energy saving and emission reduction, and promoting sustainable development. On the other hand, numerous thick wall structures with bulky dimensions and complex connection constructions have been applied into special engineering such as islands, tunnels, and deep sea projects. The precast structure is an open and complex system with a certain level of systematic risk for the whole life cycle. Moreover, structural mechanics and reliability, construction uncertainty, and resilience of precast thick wall structures still need to be revealed. For promoting the application of building industrialization to thick wall structures, nonlinear finite-element analyses on two types of large-thickness precast shear walls have been carried out based on original structural design specifications. The reinforcement connection configurations and the shear performance in terms of the load–displacement curve, lateral stiffness, ductility, energy dissipation capacity of shear walls with cast-in-place (CIP) belts, or grouting sleeves have been analyzed in detail. Numerical results show that the shear performance of two large-thickness precast shear walls is comparable to that of CIP walls. The relative error of the peak load is less than 10% for three specimens in flexural failure mode. The yield load of shear walls is relatively large and the stage between yield and failure is satisfactory. The shear performance of shear walls decreases slowly after reaching its peak value. Meanwhile, we have conducted the qualitative analysis of structural reliability for large-thickness precast shear walls in component production, quality inspection, wet work, and shear performance.

Author keywords: Building industrialization; Structural reliability; Large-thickness; Precast shear wall; Shear performance; Construction uncertainty.

Introduction

Precast reinforcement concrete (RC) shear wall structures are a type of structural systems with components suitable for industrial fabrication, which have the advantages of improving component quality, accelerating site construction, reducing construction waste, saving materials (Chen et al. 2022; Jalali et al. 2022), and reducing construction noise (Ahmed and Aziz 2019; Li et al. 2021c; Alshaikh et al. 2022). These precast RC walls have attracted attention in recent decades. However, experimental studies on precast walls are insufficient compared with those cast-in-place (CIP) walls (Chen et al. 2019a). The existing studies on precast RC structure mainly focuses on the shear performance and connection methods for precast components (Aloisio et al. 2021; Lu et al. 2021; Zhang et al. 2022b).

The utilization of unbonded post-tensioned (UPT) precast RC walls as the primary lateral load resisting system in seismic zones has been investigated. Sritharan et al. (2015) proposed the PreWEC system including UPT precast shear walls and two end columns. The end column and the precast shear wall were connected by a low-cost vertical energy dissipation connector. The study indicates that the system has satisfactory seismic performance. Lu et al. (2018) conducted a shake-table test under a series of bidirectional earthquake excitations with increasing intensity on the 1/3-scale model of a five-story self-centering RC frame with shear walls. The results demonstrate that seismic performance of the test specimen is satisfactory in the plane of the shear wall. However, the structure sustained interstory drift levels up to 2.45%. Bai et al. (2021a) investigated the nanosecond laser shock peening to improve the life-cycle performance of high-strength steels. The method has remarkable benefits for preventing life-cycle failure of large engineering structures in critical environments. Bai et al. (2021b) studied the low cycle fatigue failure of high-strength circular steel pipe concrete beams and columns under nonstationary loading. Gu et al. (2019) proposed self-centering RC shear walls with partially unbonded mild steels and conducted a cyclic loading test to study the seismic behavior of those shear walls. The experimental results show that the self-centering hybrid RC shear walls display better deformation ability and recentering ability. Dang et al. (2022) proposed a UPT concrete wall system with vertical energy-dissipating connection, which consists of precast wall panels, several X-shaped metal dampers, mild steel energy-dissipating

[1]Lecturer, School of Civil Engineering, Sanjiang Univ., Nanjing 210012, China. Email: fan_linzi@sju.edu.cn
[2]School of Civil Engineering, Southeast Univ., Nanjing 211189, China. Email: 1123728839@qq.com
[3]Professor, Key Laboratory of Concrete and Prestressed Concrete Structures of Ministry of Education, and National Prestress Engineering Research Center, Southeast Univ., Nanjing 211189, China (corresponding author). Email: chenyao@seu.edu.cn
[4]Professor, Key Laboratory of Concrete and Prestressed Concrete Structures of Ministry of Education, and National Prestress Engineering Research Center, Southeast Univ., Nanjing 211189, China. ORCID: https://orcid.org/0000-0003-1508-0384. Email: fengjian@seu.edu.cn
[5]Director, Creative Design Engineering Lab (Cdel), Dept. of Mechanical, Materials, and Aerospace Engineering, School of Engineering, Univ. of Liverpool, Liverpool L69 3GH, UK. Email: Pooya.Sareh@liverpool.ac.uk

bars, and PT tendons. They pointed out that the wall panels are resilient, and the cracks are only observed near the embedded plate in wall panels. Chen et al. (2019b) conducted an experimental study on the shear resistance of a new type of precast RC shear wall connected by vertical steel bars. They pointed out that the cracks generally appear under the line that connects the midpoint of the tension zone and the corner of the compression zone. However, the weak section of such a precast shear wall locates at the top of the preformed holes and cracks do not appear at the bottom of the wall. Twigden et al. (2017) conducted a series of cyclic lateral-load tests on four different UPT precast concrete wall systems, including two single rocking walls and two precast walls with end columns. These tests have indicated that tested walls exhibit excellent performance with uplift and rocking. Moreover, the wall base is slightly damaged. Bai et al. (2019) proposed a numerical model for earthquake damage and collapse of typical high-rise RC buildings considering strength degradation effects. Meanwhile, buckling of the reinforcement and crushing of the concrete should be adequately considered together with the P-Delta effect for collapse simulations. Erkmen (2021) studied seismic performance of unbonded post-tensioned steel layout of precast shear walls. The results provide a valuable reference for the practical application of unbonded post-tensioned precast concrete connections in seismic applications. Bedrinana et al. (2022) presented an experimental investigation on the performance of unbonded post-tensioning precast concrete walls subjected to fully reversed cyclic loads. Based on the experimental results, additional design recommendations are provided for the study of unbonded post-tensioning precast concrete walls.

Todut et al. (2014) conducted an experimental program to study the seismic performance of precast RC wall panels with and without openings. The study shows that precast RC walls investigated meet the requirements. In summary, cracks and shear slips at the horizontal joints of the UPT precast shear walls are small, and the elastic rebound of the unbonded prestressing tendons reduces the lateral residual deformation of the precast walls.

Researchers have conducted studies related to the application of precast shear walls instead of CIP shear walls in earthquake zones. Xia et al. (2021) proposed an in-plane composite beam-precast concrete shear wall connection, composed of composite beam, precast shear wall, and CIP joint region. The hysteresis curves of four specimens are relatively plumper presenting a pinching behavior, and the ability of precast specimens to dissipate energy is coincident with that of the CIP specimens. Li et al. (2021b) conducted an experimental study of four shear wall specimens, including one CIP integral specimen and three precast specimens. Then, they investigated the seismic performance of the proposed bolt-plate connection joint under low cyclic loading. The proposed connection joint can effectively improve the plastic deformation capacity of the precast shear wall and enhance the seismic performance and satisfy construction in the experiment. Zhang et al. (2022a) utilized two convolutional neural networks to identify the symmetry group and symmetry order of the structures, respectively. The method could be further extended and progressed to the identification of three-dimensional structural symmetry. Fan et al. (2021) studied the application of machine learning in an RC bridge from design to inspection. The study demonstrates that the machine learning method has great computing power and image processing capability for dealing with different aspects of RC bridges. Guo and Wang (2022) proposed an innovative equivalent monolithic precast shear wall, by introducing X-shaped steel plate bracings and a high ductility hidden column. The test results show that these walls present similar fully developed and widely distributed cracks, whilst the ultimate draft ratios and ductility coefficients of specimens meet the specification requirements, exhibiting good lateral resistance through ductile damage. Chen et al. (2012) studied the stress–strain behavior of a rectangular RC column confined by multiple spiral hoops under axial and eccentric compression. The results presented that the performance of the rectangular RC column confined by multiple spiral hoops is better than that of the conventional RC column. Li et al. (2019) and Lu et al. (2019), respectively, conducted experimental studies on different types of partially precast concrete shear walls by analyzing the hysteresis curve, skeleton curve, ductility, and bearing capacity of the specimens. Kang et al. (2013) proposed a precast emulative wall system, where the section area of bonded and unbonded rebars above the joint are reduced so that the plastic hinge can form inside the wall panel. Sun et al. (2019) conducted a low cyclic loading test on precast RC shear walls utilizing connecting steel frames and high-strength bolts. This precast shear wall has high bearing capacity, good ductility, and energy dissipation performance in the experiment.

Grouting sleeve connection is another option for precast RC shear walls. Xiao et al. (2021) presented an investigation of the impact of sleeve grouting defects on the seismic performance of precast concrete shear walls. They noted that grout sleeve defects adversely affect the seismic behavior when the spliced bars are in tension. Peng et al. (2016) conducted a pseudo-static test on a vertical reinforced precast shear wall using the grouting sleeve connection method. The test revealed that the ductility and energy dissipation capacity of grouting sleeve precast walls are comparable to that of the CIP walls. Henin and Morcous (2015) investigated the applications of nonproprietary bar splice sleeves for precast concrete walls. The bar splice sleeves that they have proposed can be simple and economical. Xu et al. (2017a, b) conducted a pseudo-static test on precast RC shear walls connected by single-row grouting sleeves and proposed a quasi-dynamic test on box structures with six layers precast RC shear walls. They indicated that the connection structure has favorable seismic performance. Han et al. (2022) designed 24 grouted sleeves specimens to study the effect of grouting material strength on bond strength of two forms of sleeves under monotonic tensile loading. They pointed out that the relative displacement between the rebar and grouting material was generated after the hardening stage of the tensile process. Sayadi et al. (2014, 2015) conducted an experimental study on the performance of grouting steel sleeves and glass fiber sleeves. Increasing the mechanical occlusion between the sleeve and the grouting material in the elastic section of the anchorage section of the rebar will reduce the bond strength between the rebar and the grouting material. For the modes based on the wet connection, precast shear walls of conventional dimensions are generally focused (Chen et al. 2020; Li et al. 2021a). Nevertheless, there are numerous giant and thick shear wall structures in some deep sea projects, nuclear island projects, tunnel projects, and substation projects. These structures are featured by bulky dimensions, dense reinforcement configurations, and complex connection. Consequently, it presents a big challenge to the difficulty and efficiency of the CIP construction.

Decision-making regarding the optimum construction and maintenance of civil infrastructures is a topic of paramount importance, and it is experiencing growing interest within the field of life-cycle structural engineering to scholars (Attarzadeh et al. 2017; Wang et al. 2021). Leu and Chang (2015) built a security risk assessment model for supply chain projects by building a Bayesian network based on fault tree transformation. In practice, appropriate preventive safety management strategies are developed to reduce the occurrence of accidents on steel building construction sites through the analysis of accident risks and significant safety factors. Mahdinia et al. (2021) adopted the fuzzy analytic hierarchy process

to develop a semiquantitative technique to assess the safety risk of construction projects. The application of this research could contribute to reducing the risk of occupational accidents in construction work. Sabatino et al. (2016) used lifetime functions, including survivor, availability, and risk at the component and system levels, to model the time-varying impact of interventions on the performance of civil infrastructure systems using closed-form analytical expressions. Govan and Damnjanovic (2020) proposed a network-based approach for risk assessment when data is limited or unreliable. The network measure highlights the relative connectivity of project tasks, resources, and risk events. Hsu et al. (2019) presented a mathematical model for the design and optimization of risk-averse logistics configurations for modular construction projects under operational uncertainty. Using robust optimization, the model explains common causes of schedule deviations on construction sites, including bad weather, delivery delays, labor productivity fluctuations, and crane breakdowns. Arashpour et al. (2016) proposed a holistic risk analysis approach that assesses the integrating impact of uncertainties on completion times. Unavailability of resources, risk seeking attitudes, and workflow variability are major contributors to the risk of late completion in hybrid construction. Tong et al. (2021) collected and screened the test data of 74 shear walls and analyzed test values of the shear capacity of the specimens. Meanwhile, they adjusted the formula for shear capacity so that the reliability index calculated by the adjusted formula meets the current code's requirements. Jiang et al. (2015) built a nonlinear failure function of RC frame columns with tension failure under combined vertical and horizontal loads. The numerical simulation results indicate that the model is effective in obtaining accurate reliability results and predicting changes in reliability. Abualreesh et al. (2022) demonstrated the reliability methodology through a set of representative unsymmetrical and symmetrical RC shear wall frame buildings subjected to the El-Centro earthquake. They pointed out that that the reliability constraint is generally the controlling constraint in the optimization of shear wall frame structures subjected to seismic action.

To overcome these difficulties and guarantee the integrity of structures under shear loading, the mechanical properties of connection joints of large-thickness precast shear walls will be analyzed in this study. We have performed finite-element analysis on the shear walls with CIP belts or grouting sleeves. Meanwhile, the finite-element analysis models of CIP shear walls will be established to perform comparative analysis. The overall design concept is presented in the following section. Subsequently, experimental investigations on three specimens of shear walls are described. The results are then studied and discussed, followed by the conclusion of the paper.

Design Overview

The wet connection requiring wet work on site involves grouting cement-based material into the wall, to anchor the reinforcement cage. At present, the wet connection mainly includes the grouting sleeve connection, constraint grout-filled lap connection, vertical reinforcement cluster connection, CIP belts connection, and connection with the precast double-side superimposed shear wall. Here, we have analyzed mechanical properties of connection joints for large-thickness precast shear walls. Based on three-dimensional models of RC shear wall structures, we evaluate the feasibility and reliability of the fabricated construction. As shown in Figs. 1–3, simple three-dimensional models of the CIP shear wall, shear wall with CIP belts, or grouting sleeves have been established. Note that, in Figs. 1–3, the rebars are denoted by C, where C10 represents grade HRB400 (design value of strength $f_y = 360$ N/mm^2) rebars of 10 mm in diameter.

The wet connection methods for several large-thickness precast shear walls have been analyzed and compared, as listed in Tables 1 and 2. Noteworthy, the connection modes S1–S6 denote grouting sleeves connection, constraint grout-filled lap connection, vertical reinforcement cluster connection, CIP belts connection with direct lap, CIP belts connection with U-shaped hoop lap, and connection with precast double-side superimposed shear wall, respectively.

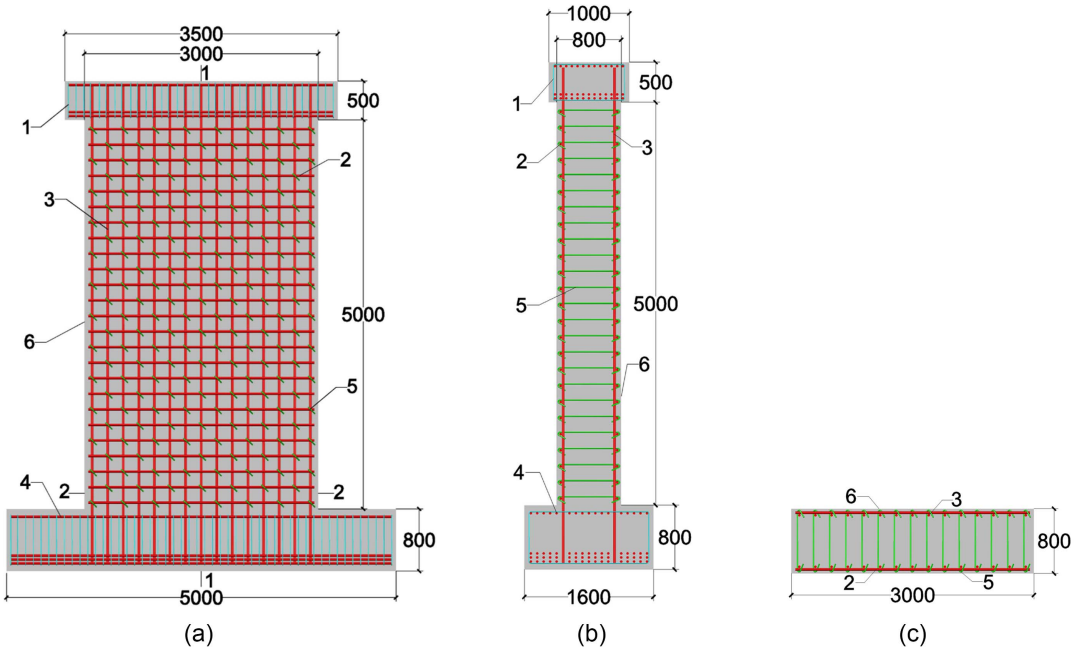

Fig. 1. Cast-in-place shear wall: (a) front view; (b) section 1-1; and (c) section 2-2. 1-C10@100; 2-C32@200; 3-C32@200; 4-C32; 5-C16 (200 × 400); and 6-CIP concrete.

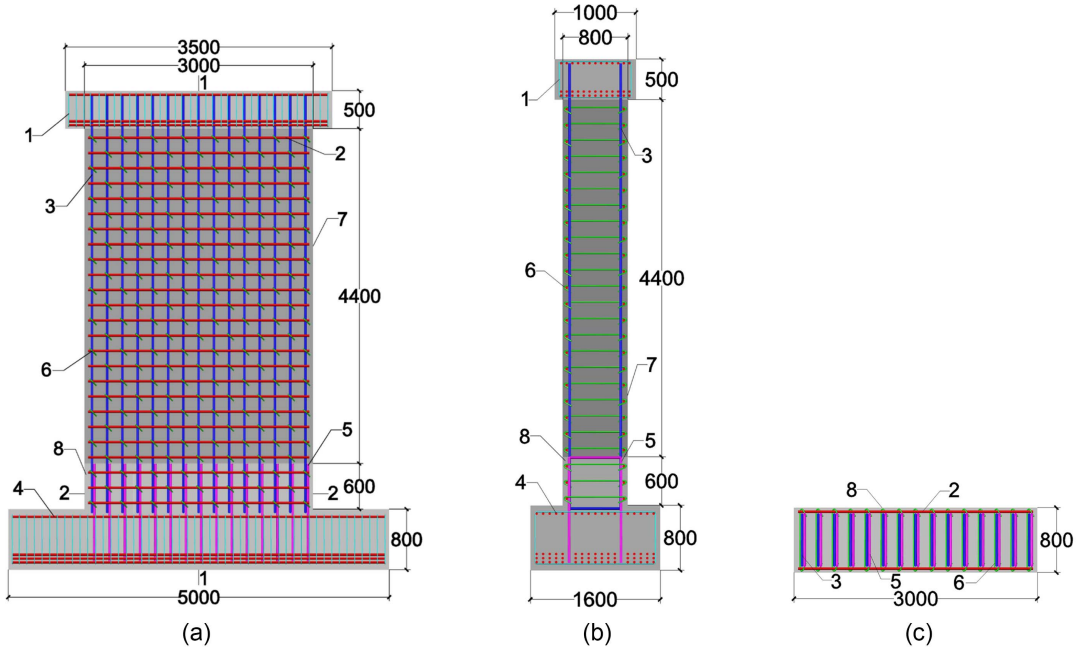

Fig. 2. Shear wall with cast-in-place belts: (a) front view; (b) section 1-1; and (c) section 2-2. 1-C10@100; 2-C32@200; 3-C32@200; 4-C32; 5-C32@200; 6-C16(200 × 400); 7-precast wall; and 8-CIP concrete.

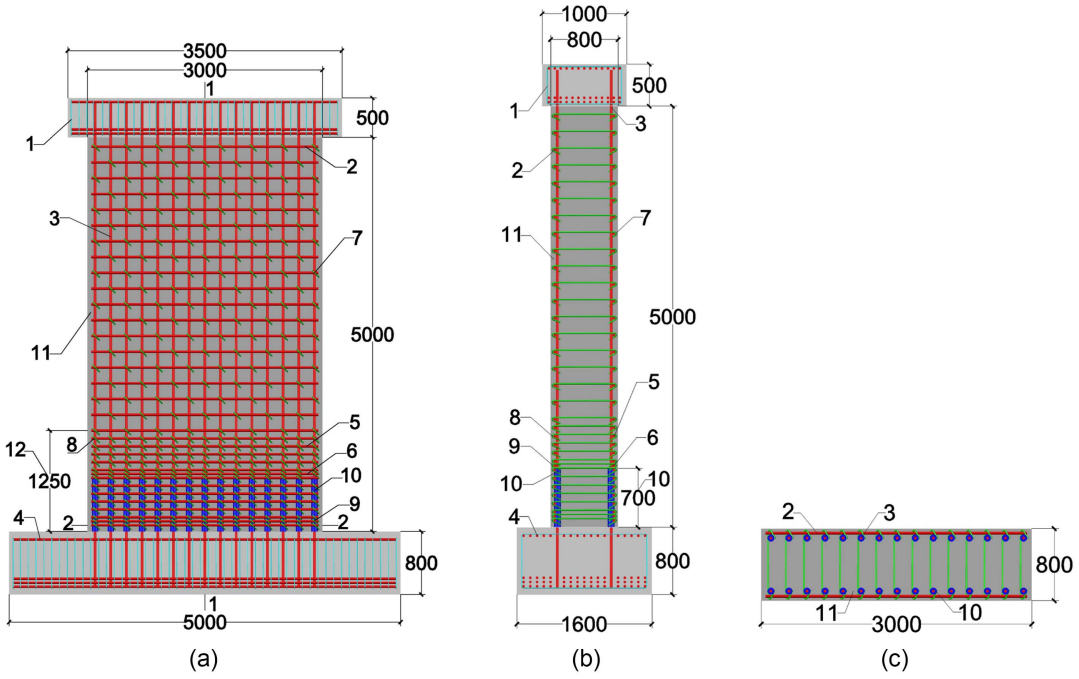

Fig. 3. Shear wall with grouting sleeves: (a) front view; (b) section 1-1; and (c) section 2-2. 1-C10@100; 2-C32@200; 3-C32@200; 4-C32; 5-C32@200; 6-C32@50; 7-C16(200 × 400); 8-C16(100 × 200); 9-C16(50 × 100); 10-steel sleeves (d = 80 mm); and 11-precast wall.

Table 1. Connection modes with reserved holes (mm)

Connection mode	Anchor length	Sleeve length	No. of sleeves	Cross-sectional diameter	Spacing of sleeves	Densified area of horizontal rebar
S1	640	700	30	80	200	1,250
S2	1,909	1,960	15	100	400	2,000
S3	1,909	1,960	4	200	600	2,000

Table 2. Connection modes with reserved back pouring belt (mm)

Connection mode	Length of post pouring section	Thickness of post pouring section	Height of post pouring section	Rebar bending length	Lap length
S4	3,000	800	1,200	—	1,458
S5	3,000	800	600	604	729
S6	3,000	400	5,000	—	1,431

As presented in Table 1, the length of the sleeve/channel for the connection modes S2 and S3 approach 2 m. Thereafter, the involved on-site construction would be rather difficult. For the mode S3, the diameter of longitudinal rebars is 32 mm. Manual bending on these rebars becomes difficult for effective on-site construction. Consequently, a partition wall would be required to reduce grouting resistance and achieve better grouting efficiency.

As presented in Table 2, the lap length of the reinforcements for the connection S4 is much larger, and the upper components are difficult to be fixed and constructed on site. Method S5 can effectively reduce the lap length of the reinforcement. However, bending 32-mm-diameter rebars into U-shaped hoops still demands machinery. Meanwhile, concrete placement at the top of the CIP belt zone is prone to unconsolidation. Method S6 can resolve the superstructure fixation difficulties without additional formwork support. Internal rebar trusses would affect concrete placement, so self-compacting concrete or concrete with a maximum particle size of less than 25 mm can be utilized. Meanwhile, the fabrication of the components in method S6 is sophisticated, such as connecting of internal and external leaf walls, binding of internal rebar trusses, and inserting of insulated components.

Finite-Element Modeling

Specimens Description

The shear wall specimens have been designed by the national standards GB 50010-2010 (CS 2010a) and GB 50011-2010 (CS 2010b) for the construction industry in China. Moreover, they meet the relevant design provisions in the standards JGJ-1-2014 (CS 2014) and GB 51231-2016 (CS 2016). To comprehensively study the load response and shear resistance of large-thickness precast shear walls, finite-element analyses were conducted on three specimens under monotonic loading. Noteworthy, the walls WA, WB, and WC denote the CIP shear wall, shear wall with CIP belts, and shear wall with grouting sleeves, respectively. The cross-sectional parameters and reinforcement configurations of specimens have been shown in Figs. 1–3. We disassemble the shear wall units and set the cross-sectional dimensions of the specific components. In transverse direction, the loading beam connecting with the shear wall have a section of 3,500 × 1,000 mm, and the foundation beam is 5,000 × 1,600 mm. The cross-sectional dimension of the whole wall is 3,000 × 800 mm with a height of 5,000 mm. The concrete strength grade is C40, whereas $f_c = 19.1\ \mathrm{N/mm^2}$, and $f_t = 1.71\ \mathrm{N/mm^2}$. Reinforcement adopts HRB400 grade, with $f_y = 360\ \mathrm{N/mm^2}$. We use u to replace the design axial compression ratio.

Finite-Element Models

As shown in Fig. 4, we consider the shear wall with CIP belts as an example to establish the finite-element model utilizing ABAQUS version 6.14 software. The reinforcement is embedded into the concrete. The concrete and reinforcement are meshed by C3D8R solid elements and T3D2 truss elements, respectively. Constraints on displacement and rotation are imposed at the base of the foundation beam in the x-, y-, and z-directions, which is taken to be fixed. The gravity is exerted first, then a uniform vertical pressure load is exerted on the loading beam. Finally, a horizontal load is exerted on the loaded beam by means of displacement loading.

Ideal elastoplastic and plastic damage constitutive models are used for reinforcement and concrete, respectively. The material properties of the reinforcement and concrete damage constitutive models are established by the standard GB50010-2010. The loading beam of WB is modeled integrally with the precast wall to achieve a rigid connection. The normal direction of the contact surface is simulated by "hard contact," while the tangential direction is simulated by a combination of "interface-based bonding behavior" and the Coulomb friction criterion. Both K_{ss} and K_{tt} are the ratio of concrete shear modulus to unit displacement, and K_{nn} is the ratio of concrete elastic modulus to unit displacement. We specify

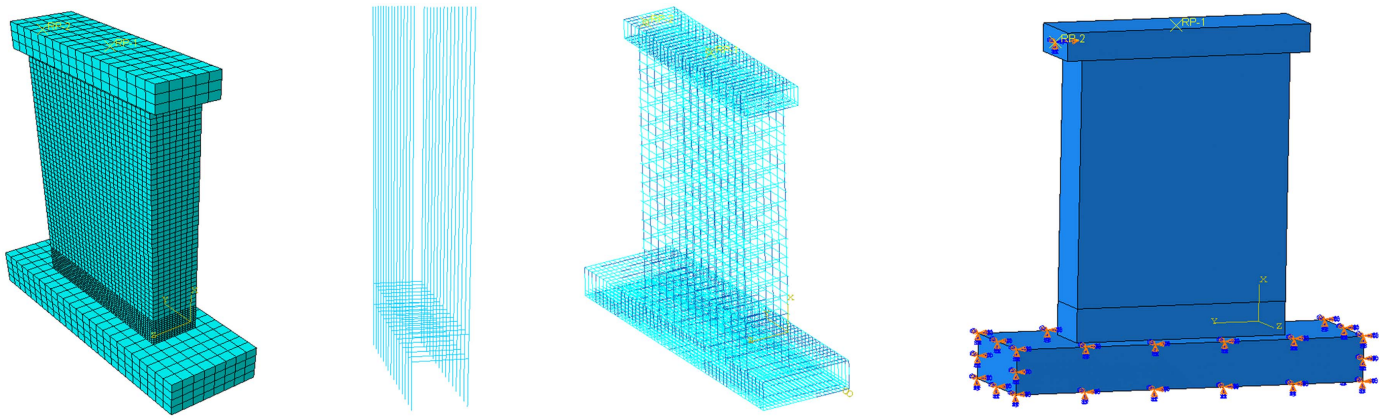

Fig. 4. Finite element model of WB: (a) concrete model and meshing; (b) u-shaped rebar model; (c) rebar model; and (d) boundary condition.

$K_{ss} = 13{,}000$, $K_{tt} = 13{,}000$, and $K_{nn} = 32{,}500$. Sleeves of WC are crafted from mild steel, which has a greater intensity than reinforcement. The area of the steel in the cross section of the connection segment is calculated using an equal section of steel in place of the sleeve. Sleeves are embedded in the concrete together with rebars to fulfill the calculation requirements. Similarly, a contact surface exists between the precast concrete and foundation beam. Hard contact is adopted in the normal direction of the contact surface, and the Coulomb friction criterion is adopted in the tangential direction with a friction coefficient of 0.3.

Finite-Element Analysis Results

WA: Cast-in-Place Shear Wall

Concrete Stress

The shear performance of large-thickness precast shear walls has been investigated applying a horizontal load on specimens along the x-direction. The horizontal load has been applied by displacement loading with a final load value of 200 mm. The stress in the x-direction of the concrete unit is expressed by S11. It shows the accumulation of concrete stress during the whole loading process, which can intuitively reflect the plastic deformation of specimens and development of cracks. As shown in Fig. 5, the final stress diagrams of concrete are obtained by exerting a bidirectional load on the wall WA. The stress distribution of concrete under horizontal load is mainly concentrated in the corner of the wall. The phenomenon is attributable to the integral pouring between the wall and foundation of the CIP shear wall. During an earthquake, the wall will shake with the foundation and the corner of the wall is subjected to repeated action of tension and pressure. As u increases, the stress on the specimen gradually increases.

Tensile and Compressive Damage of Concrete

Combining with the strain of rebars, the yield displacement, peak displacement, ultimate displacement, and corresponding load have been obtained for each model. The yield displacement is the horizontal displacement of rebars when they begin to yield. When the ultimate load is 85% of the peak load, the specimen has been damaged. We have analyzed the plastic damage of concrete in various stages. The tensile and compressive damage are represented by DAMAGET and DAMAGEC, respectively. In Fig. 6, the tensile and compressive damage of specimens have been depicted under conditions of axial compression ratios of 0.2 and 0.3.

As shown in Fig. 6, the tensile damage is primarily concentrated in the lower-left corner and the middle of the wall. Tensile horizontal cracks emerge first in the region where the lower-left corner of the wall intersects the foundation beam. As the load increases, the horizontal cracks migrate upward, while inclined cracks emerge at the top left of the specimen. The compressive damage begins at the lower-right corner of the specimen and gradually expands toward the compression zone at the loading terminal. With the increment of displacement, the compressive damage of gradually expands. Ultimately, compressive damage reaches a maximum in the lower-right region of the wall at the connection with the foundation beam.

Rebar Stress

By analyzing the rebar stress in different locations, we could determine the stress state of shear walls, transfer path of force flow inside shear walls, and force transmission pattern at connection joints from a macroscopic point of view. This contributes to the preliminary understanding of the shear resistance mechanism of large-thickness precast shear walls. Fig. 7 presents the stress of rebars under axial compression ratios of 0.2 and 0.3. The tensile and compressive stress are expressed as positive and negative value, respectively.

In the cracking stage, the longitudinal reinforcement in both sides of the wall commences to be stressed. The stress distributed in distributed rebars and stirrups is low while the reinforcement remains elastic. Part of reinforcement yields in the extreme stage. As cracks develop, the stress in the reinforcement distributed along diagonal cracks increases rapidly. Finally, the longitudinal reinforcement in both sides and middle of the wall along the direction of the diagonal crack yield.

WB: Shear Wall with Cast-in-Place Belts

Concrete Stress

As shown in Fig. 8, the final stress diagrams of concrete have been obtained by exerting a bidirectional load on the wall WB. The concrete in the lower-right corner of WB is severely broken and has a propensity to develop diagonal connecting cracks. A slight misalignment between the CIP and precast section can generate interfacial stress concentrations. The stress distribution under the load is primarily concentrated in the lower-right corner of the wall. Although the stress is slightly higher at the joint between the CIP and precast section, they work well together.

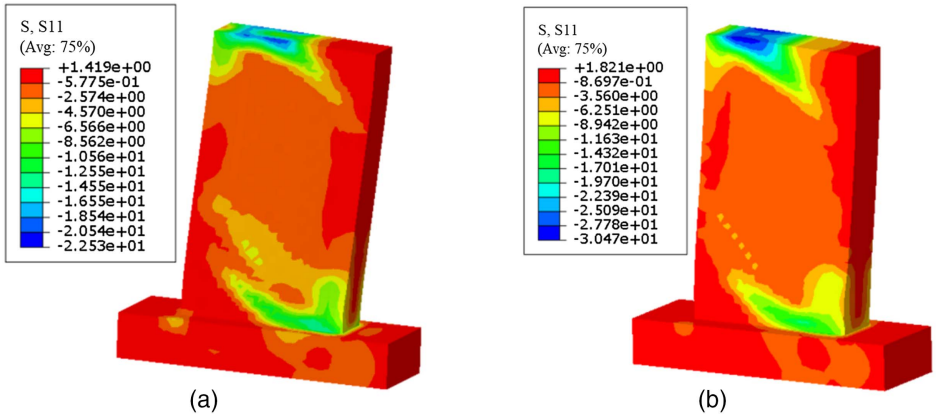

Fig. 5. Concrete stress: (a) $u = 0.2$; and (b) $u = 0.3$.

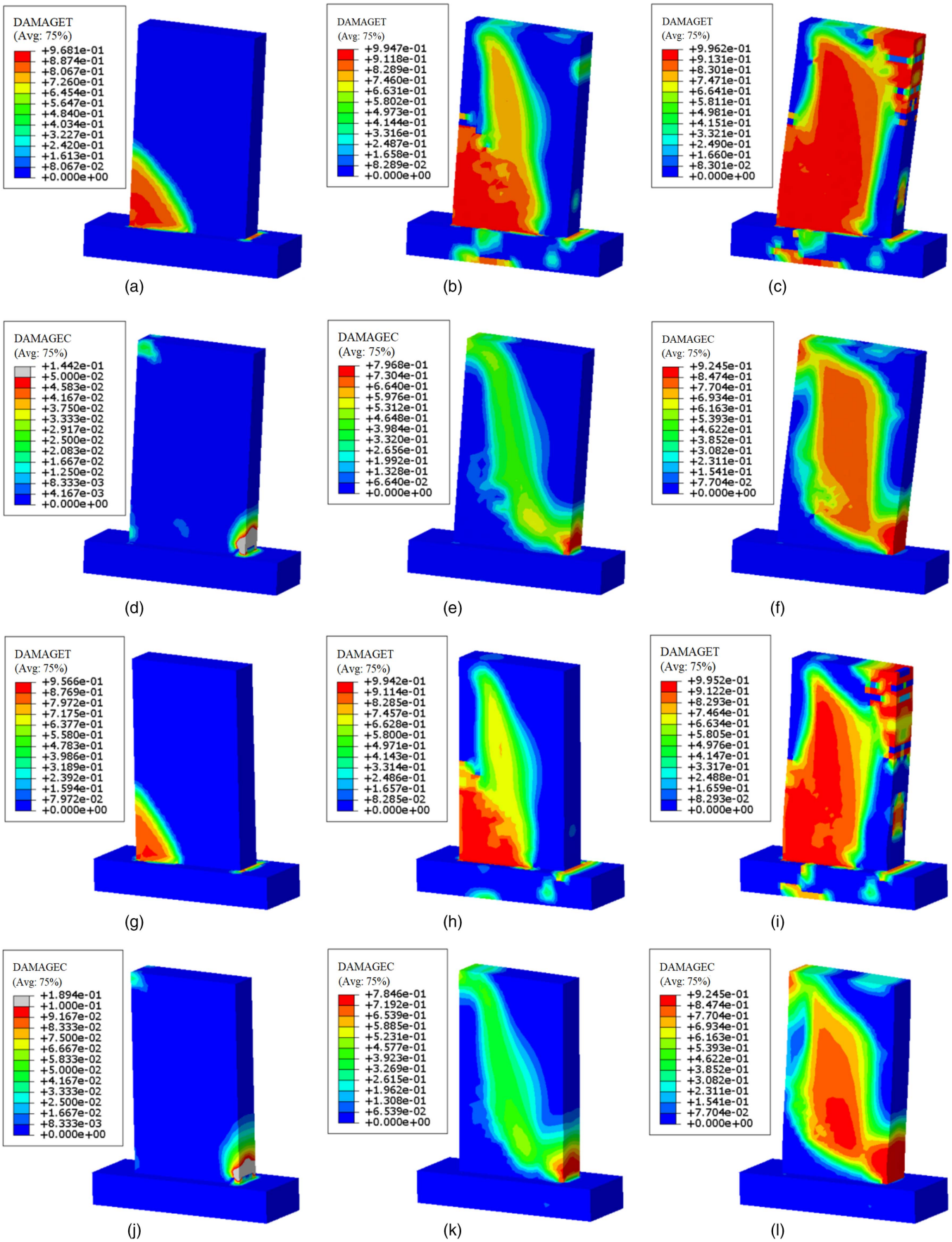

Fig. 6. Tensile and compressive damage of wall WA: (a and d) displacement loading 7 mm; (b and e) peak load ($\Delta = 40.19$ mm); and (c and f) ultimate load ($\Delta = 104.74$ mm) axial compression ratio $u = 0.2$; and (g and j) displacement loading 7 mm; (h and k) peak load ($\Delta = 34.51$ mm); and (i and l) ultimate load ($\Delta = 96.79$ mm) axial compression ratio $u = 0.3$.

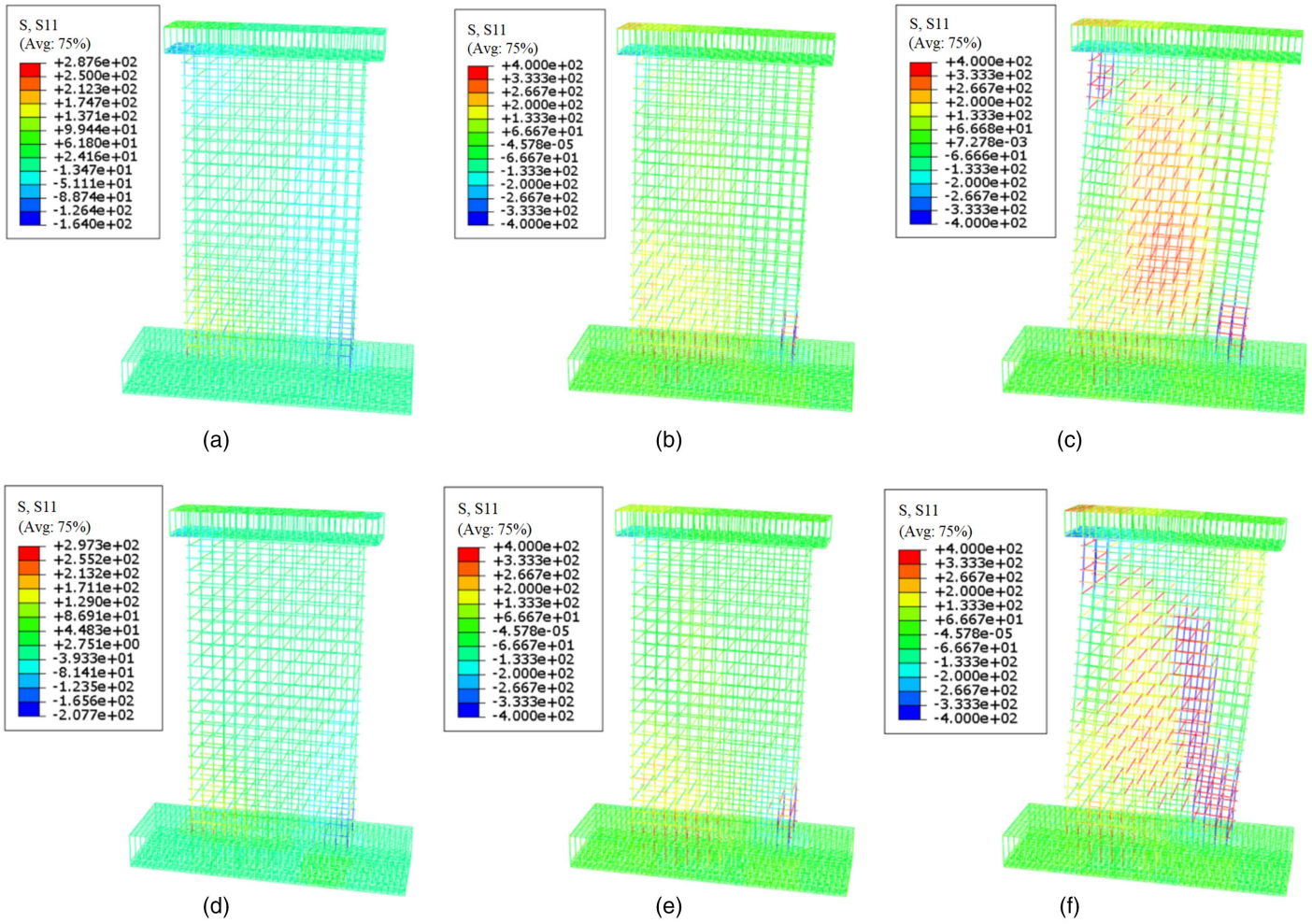

Fig. 7. Rebar stress of wall WA: (a) cracking stage; (b) extreme stage; and (c) destruction stage axial compression ratio $u = 0.2$; and (d) cracking stage; (e) extreme stage; and (f) destruction stage axial compression ratio $u = 0.3$.

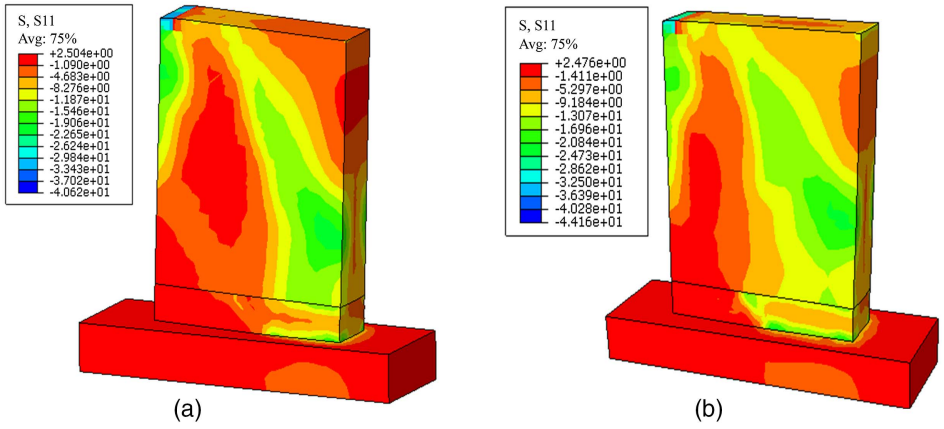

Fig. 8. Concrete stress of wall WB: (a) $u = 0.2$; and (b) $u = 0.3$.

Tensile and Compressive Damage of Concrete

In Fig. 9, the tensile and compressive damage of specimens have been depicted under conditions of axial compression ratios of 0.2 and 0.3. Tensile horizontal cracks first emerge in the junction zone between the precast and CIP sections of the wall. The concrete is critically stretched and cracked within 600 mm height in the tensile corner zone of the wall WB. The stirrups and horizontal distribution rebars are exposed, and part of the concrete exits the work. The appearance of tensile horizontal cracks indicates that most of the stirrups and tensile rebars in the junction zone yield, and the shear performance of the component decreases. As displacement increases, cracks gradually penetrate the lower-left wall.

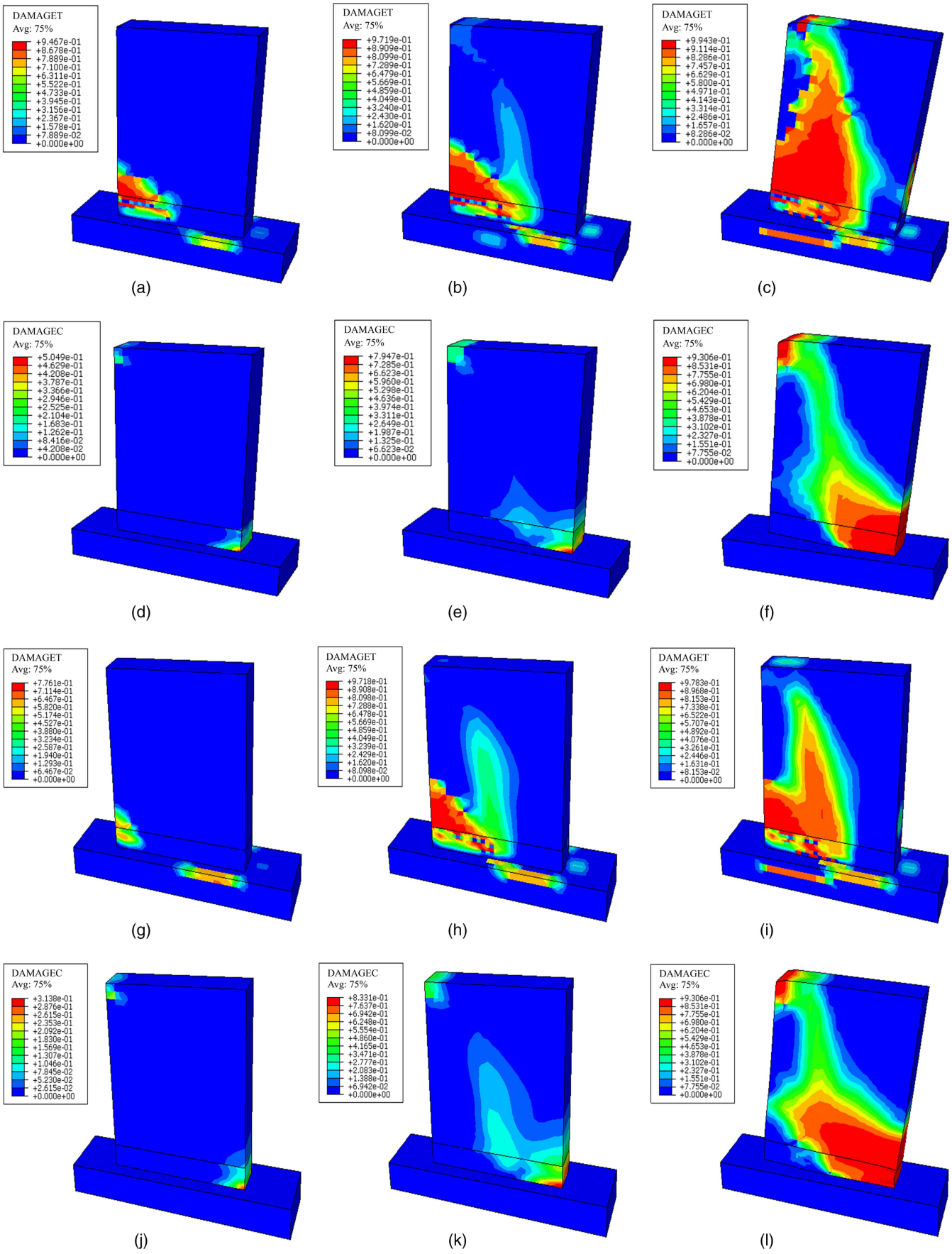

Fig. 9. Tensile and compressive damage of wall WB: (a and d) displacement loading 7 mm; (b and e) peak load ($\Delta = 35.82$ mm); and (c and f) ultimate load ($\Delta = 81.42$ mm) axial compression ratio $u = 0.2$; and (g and j) displacement loading 7 mm; (h and k) peak load ($\Delta = 36.04$ mm); and (i and l) ultimate load ($\Delta = 70.15$ mm) axial compression ratio $u = 0.3$.

Subsequently, tensile horizontal cracks gradually migrate upward, while developing into oblique cracks toward the upper-left side of the wall. As load increases, the compressive damage of the wall gradually progresses from the lower-right side to the middle of the wall. The cracks distribute widely; hence, the wall can adequately dissipate energy when the load is imposed.

Rebar Stress

Fig. 10 presents the stress of rebars under axial compression ratios of 0.2 and 0.3. The tensile and compressive stress are expressed as positive and negative value, respectively. Precast and CIP segments of the wall WB depend on anchor connections of u-shaped rebars to implement common load bearing. The wall has good ductility when the u-shaped rebars are deeply embedded, effectively reducing the crack width. Simultaneously, u-shaped rebars could be applied as a restraining edge member of the wall, acting as a positioning element during construction and making the connection reliable. The deformation of rebars at the connecting seam is extensive, which can withstand certain loads. In the destruction stage, the longitudinally stressed rebars in both sides of the wall yield. As u becomes larger, the greater the yield area and deformation of the reinforcement.

WC: Shear Wall with Grouting Sleeves

Concrete Stress

As shown in Fig. 11, the final stress diagrams of concrete have been obtained by exerting a bidirectional load on the wall WC.

The wall WC depends on interior longitudinal reinforcement and steel sleeves to convey loads, and concrete in the bottom and upper pressure zones is crushed to form a through joint section. The concrete cracks are densely developed at the tensile end of the wall. In general, cracks with maximum width locate at the top of the preformed holes, which are usually the first cracks induced by the rising horizontal load. Damage forms of both the wall WC and the wall WA are flexural failure.

Tensile and Compressive Damage of Concrete

Fig. 12 depicts the tensile and compressive damage of specimens under conditions of axial compression ratios of 0.2 and 0.3. Several diagonal cracks emerge in the middle of the wall because of the distribution of tension stress flow. It starts from the tensile side and ends at the corner of the compressive side. Cracks in the tensile zone are primarily horizontally distributed. The presence of precast steel sleeves could generate a static mutations phenomenon. As u increases, the tensile and compressive damage of the specimen also increases and reaches the failure state in advance.

Rebar Stress

In Fig. 13, the stress of rebars has been presented under axial compression ratios of 0.2 and 0.3. The tensile and compressive stress are expressed as positive and negative value, respectively. In the extreme state, the longitudinal stressed reinforcement in both sides of the wall partially yields, which is consistent with the flexural damage of specimens. Lack of restraint of concrete after horizontal seam cracking increases the strain on the reinforcement. In the destruction stage, the reinforcement at the bottom of tensile zone

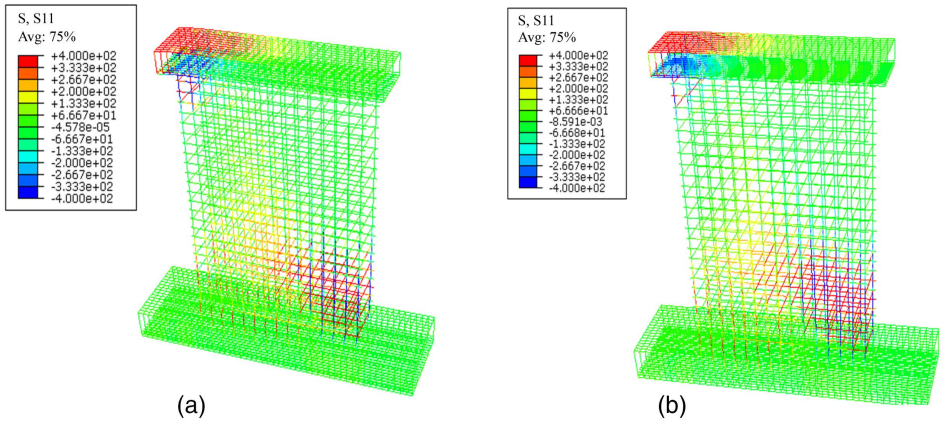

Fig. 10. Rebar stress (destruction stage) of wall WB: (a) $u = 0.2$; and (b) $u = 0.3$.

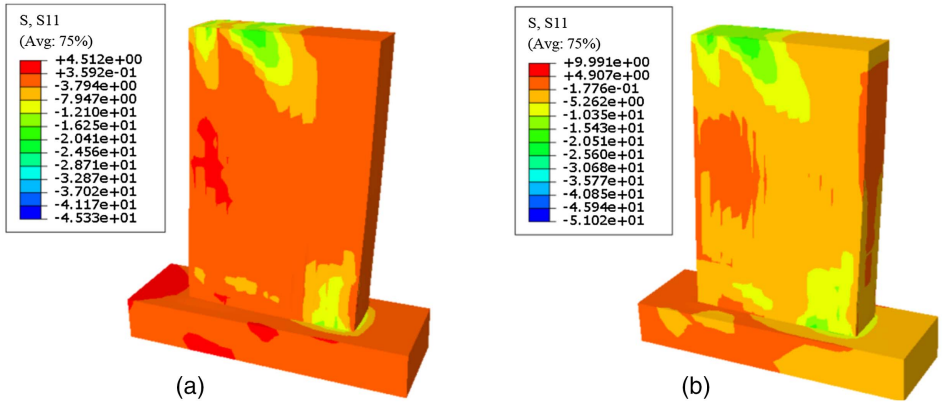

Fig. 11. Concrete stress of wall WC: (a) $u = 0.2$; and (b) $u = 0.3$.

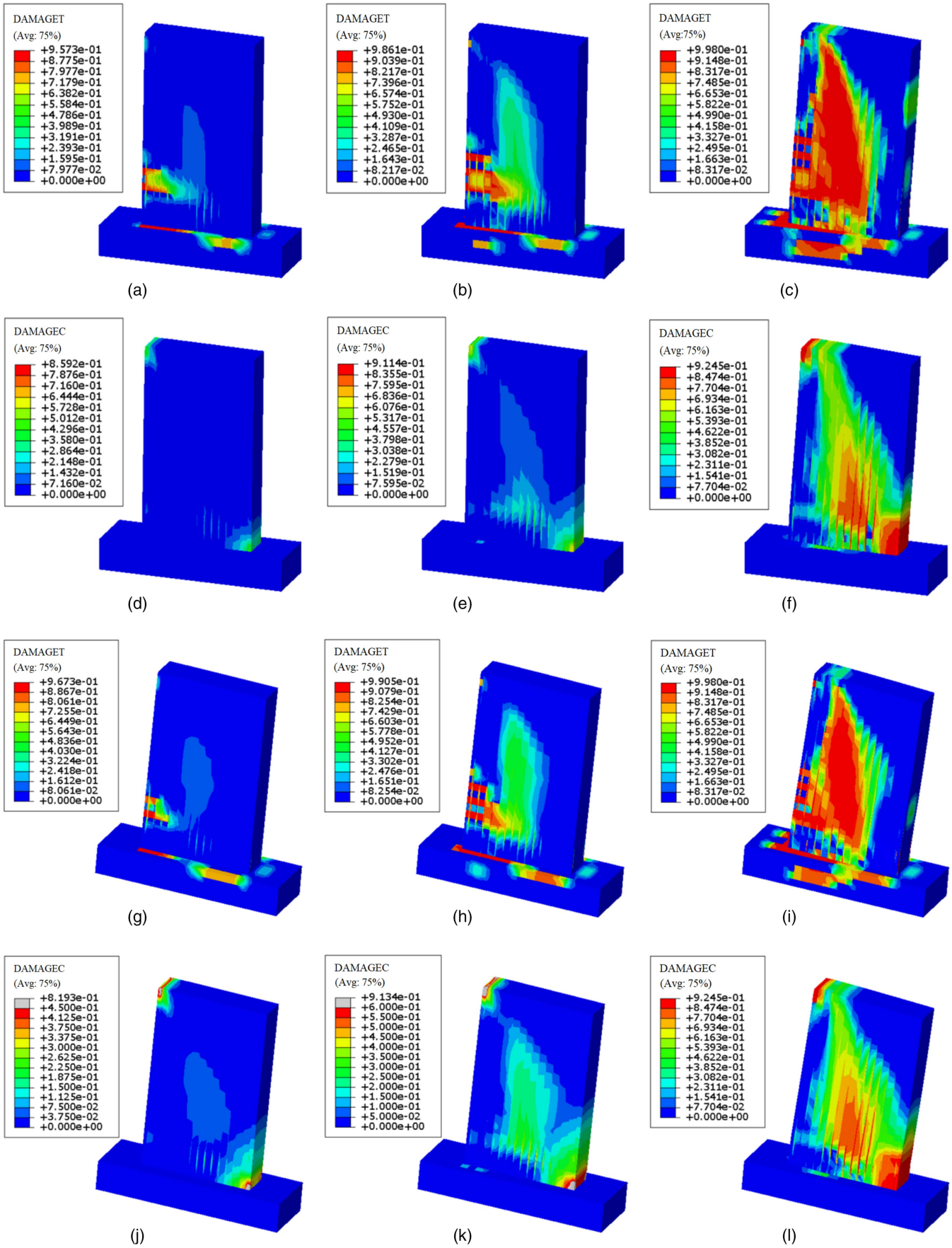

Fig. 12. Tensile and compressive damage of wall WC: (a and d) displacement loading 7 mm; (b and e) peak load ($\Delta = 24.51$ mm); and (c and f) ultimate load ($\Delta = 90.35$ mm) axial compression ratio $u = 0.2$; and (g and j) displacement loading 7 mm; (h and k) peak load ($\Delta = 26.70$ mm); and (i and l) ultimate load ($\Delta = 82.71$ mm) axial compression ratio $u = 0.3$.

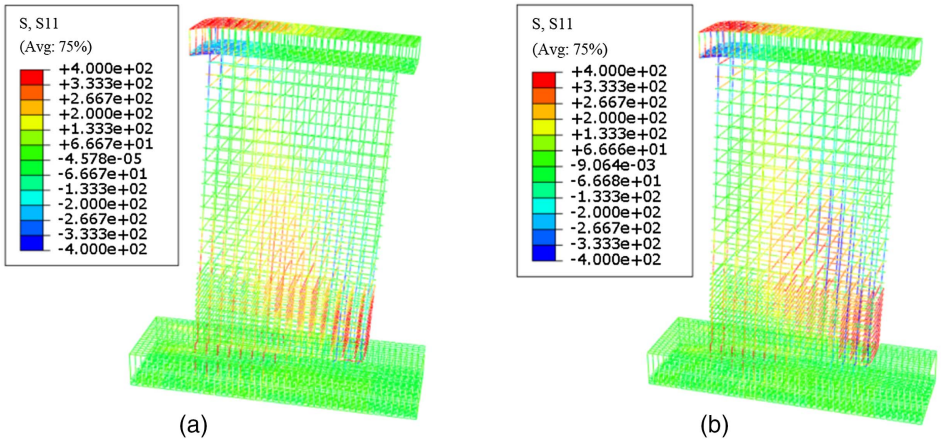

Fig. 13. Rebar stress (destruction stage) of wall WC: (a) $u = 0.2$; and (b) $u = 0.3$.

yields. Stress concentration of reinforcement will emerge from the horizontal seam. The maximum stress in the reinforcement emerges at the bottom of the tensile component and the lower end of the sleeves.

Summary of Large-Thickness Precast Shear Walls

The precast structure has the advantages of energy-saving, green and environmental protection, and has a broad development prospect. Nevertheless, promoting the application of large-thickness precast shear walls in the building industrialization requires a more intensive and comprehensive evaluation.

1. There is arch, beam, and suspension line mechanisms in the precast structure during progressive collapse, and each force mechanism exists the problems of compounding and transformation. Hence, the design and calculations for antiprogressive collapse should concentrate on the form of joint seams, initial defects, and overall stability.
2. The beam–column joints cannot be guaranteed to be completely rigidly connected during the actual construction. Furthermore, the component production and large amount of wet work on site could lead to the construction uncertainty. When the connection joints are subjected to extreme loads, the deformation of the precast structures has uncertainty.
3. The precast structure has a multitude of joint seams, which are prone to stress concentrations. This phenomenon could generate cracks or even damage to structures and reduce the seismic performance of precast structure.
4. The precast structure is an open and complex system with a certain level of systematic risk for the whole life cycle. Meanwhile, policies and regulations, market environment, and technology level will bring more uncertainty to project cost control.

In summary, compared with the CIP structure, the reliability, antiprogressive collapse, and seismic resistance of the precast structure are slightly weaker. Thus, engineers need to pay more attention in the design and structural analysis of the precast structure.

Discussion and Conclusions

The load–displacement curve can indicate shear performance of precast RC walls. By analyzing the load–displacement curve, we can not only understand the stiffness degradation of the specimen, but also distinguish the elastic and elastoplastic properties of the specimen under the horizontal load. The load–displacement parameters of the critical joints of specimens have been presented, as listed in Table 3. Noteworthy, D and L denote displacement and load, respectively. The ultimate displacement of WA exceeds that of WB and WC by over 10%, indicating the best ductility. From the peak load to the ultimate load state when $u = 0.2$, the displacement of WA, WB, and WC has increased by 64.55, 45.6, and 65.84 mm, respectively. WB has a smaller displacement increase compared with the other shear walls; it has less stiffness and poor ductility. The disparity between the peak load of WA and WC is less than 5% at different u.

As observed from Fig. 14, we have compared the load–displacement curves of three specimens. The shear resistance process of precast walls undergoes several typical stages. At the initial stage of loading, each specimen maintains in the elastic stage. Because the wall is undamaged, the load–displacement curve is approximated as a straight line. Subsequently, the reinforcement in the tensile region of the wall commences to yield. With the increase of plastic deformation and the development of cracks, the bearing capacity of walls reaches the peak. Eventually, top displacement increases rapidly due to the substantial loss of bearing capacity, and the specimen has entered the failure phase.

Shear performance is an important evaluation indicator for large-thickness precast shear walls, but the efficiency in the construction

Table 3. Load and displacement parameters of key joints

u	Serial No.	Yield, D (mm)	Yield, L (kN)	Peak, D (mm)	Peak, L (kN)	Ultimate, D (mm)	Ultimate, L (kN)
0.2	WA	8.75	5,565.3	40.19	8,160.9	104.74	6,955.0
	WB	10.91	5,413.2	35.82	7,996.2	81.42	6,786.7
	WC	14.2	6,941.0	24.51	8,112.1	90.35	6,982.1
0.3	WA	9.89	6,822.5	34.51	9,299.5	96.79	7,907.6
	WB	7.50	7,410.0	36.04	8,930.1	70.15	7,577.7
	WC	10.72	7,346.1	26.70	8,881.9	82.71	7,549.6

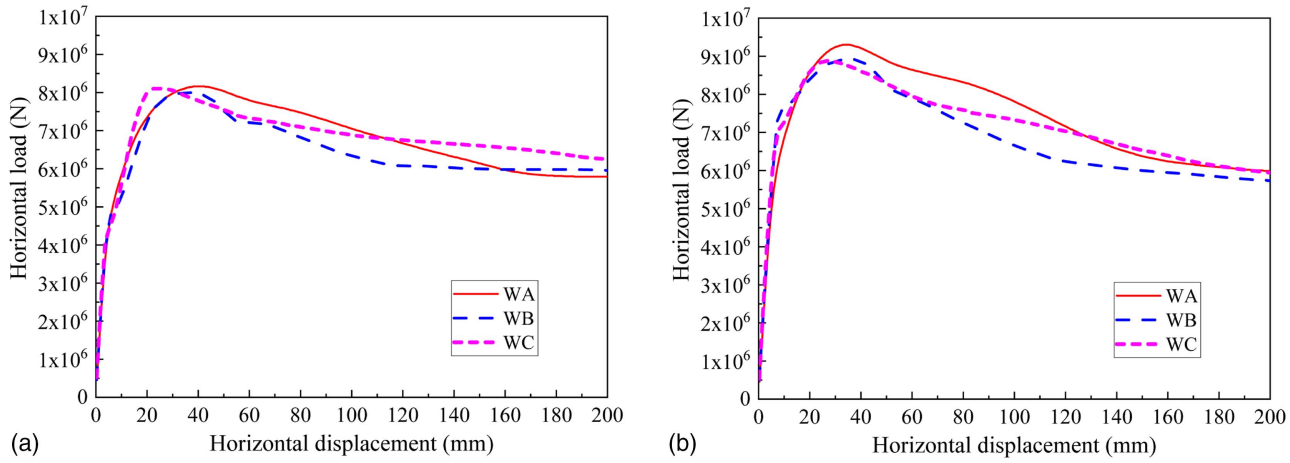

Fig. 14. Load–displacement curve of different shear walls: (a) $u = 0.2$; and (b) $u = 0.3$.

Table 4. Comparison for wet connection methods

Serial No.	Component production	Wet work	Additional rebars	Construction difficulty	Economic cost	Quality inspection	Shear performance
S1	Easy	Small	Small	Easy	Low	Harder	Fine
S2	Easy	Smaller	Large	Hard	Lowest	Harder	—
S3	Hard	Larger	Smaller	Hardest	High	Hard	—
S4	Harder	Large	Large	Harder	Low	Easy	—
S5	Harder	Large	Large	Harder	Low	Easy	Fine
S6	Hardest	Largest	Larger	Easier	Higher	Easier	—

process should also be considered. For example, the length of the sleeves approach 2 m for vertical reinforcement cluster connection, which poses a huge challenge to the construction of large-thickness precast shear walls. According to the research results, we have conducted the qualitative analysis of structural reliability for large-thickness wet connection methods. The comparison has been presented, as listed in Table 4. Structural reliability is significant for assessing the overall performance of large-thickness precast structures. For example, compared to the connection S6, S1 has a lower economic cost and easier component production. Simultaneously, S6 is less difficult to construct due to the smaller wet work on site, thus contributing to the overall structural reliability. The reliability design of the structure is usually based on the reliability of the components. We could normally compare structural reliability based on the component production, additional rebars, wet work, and shear performance to determine the optimal connection scheme of S1–S6. Damage to one component or cross section in earthquake-resistant structures does not signal the destruction or collapse for the whole structures. The precast structure enters a nonlinear state under heavy earthquake and the performance of components deteriorates, leading to a decrease in the bearing capacity and systemic reliability. Thus, the selection of proper large-thickness precast shear walls requires comprehensive reliability analyses.

In the present study, the authors have investigated the shear performance of large-thickness precast shear walls. On the basis of the results, certain conclusions can be drawn as follows: When the axial compression ratio of three specimens is 0.3, good bearing capacity, ductility, and energy dissipation can be obtained. From the failure mode, the plastic distribution area of the main wall is larger, which is an important characterization of the shear energy dissipation.

1. The precast shear walls proposed in this paper have good assembling and force performance in terms of ensuring reliable load transfer. The damage mode and ultimate load are determined by the connection configuration of the main wall. The destruction mode of each specimen is a bending-shear failure.
2. Each precast wall will undergo three typical stages in shear resistance: elasticity, yielding, and failure. It is a long process from the yielding to the failure stage, and the shear performance decreases slowly after the load exceeds the peak value. Results show that the shear performance of two precast shear walls is comparable to that of CIP. Therefore, they could be promoted for application to thick wall structures.

Data Availability Statement

All data, models, or code that support the findings of this study are available from the corresponding author upon reasonable request.

Acknowledgments

This work was supported by the National Natural Science Foundation of China (Grant Nos. 51978150 and 52050410334), the Fundamental Research Funds for the Central Universities, and the Natural Science Foundation of the Jiangsu Higher Education Institutions of China (Grant No. KZ2022043). Note that the authors Fan and Wei contributed equally to this work. The authors are grateful to the editors and anonymous reviewers for their professional comments and valuable suggestions that led to the improvement of the quality of the paper.

References

Abualreesh, A. M., A. Tuken, A. Albidah, and N. A. Siddiqui. 2022. "Reliability-based optimization of shear walls in RC shear wall-frame buildings subjected to earthquake loading." *Case Stud. Constr. Mater.* 16 (Jun): e00978. https://doi.org/10.1016/j.cscm.2022.e00978.

Ahmed, G. H., and O. Q. Aziz. 2019. "Shear strength of joints in precast posttensioned segmental bridges during 1959-2019, review and analysis." *Structures* 20 (Aug): 527–542. https://doi.org/10.1016/j.istruc.2019.06.007.

Aloisio, A., F. Boggian, R. Tomasi, and M. Fragiacomo. 2021. "Reliability-based assessment of LTF and CLT shear walls under in-plane seismic loading using a modified Bouc-Wen hysteresis model." *ASCE-ASME J. Risk Uncertainty Eng. Syst. Part A: Civ. Eng.* 7 (4): 04021065. https://doi.org/10.1061/AJRUA6.0001161.

Alshaikh, I. M. H., A. A. Abadel, and M. Alrubaidi. 2022. "Precast RC structures' progressive collapse resistance: Current knowledge and future requirements." *Structures* 37 (Mar): 338–352. https://doi.org/10.1016/j.istruc.2021.12.086.

Arashpour, M., R. Wakefield, E. W. M. Lee, R. Chan, and M. R. Hosseini. 2016. "Analysis of interacting uncertainties in on-site and off-site activities: Implications for hybrid construction." *Int. J. Project Manage.* 34 (7): 1393–1402. https://doi.org/10.1016/j.ijproman.2016.02.004.

Attarzadeh, M., D. K. H. Chua, M. Beer, and E. L. S. Abbott. 2017. "Fuzzy randomness simulation of long-term infrastructure projects." *ASCE-ASME J. Risk Uncertainty Eng. Syst. Part A: Civ. Eng.* 3 (3): 04017002. https://doi.org/10.1061/AJRUA6.0000902.

Bai, Y., S. Guan, X. Lin, and B. Mou. 2019. "Seismic collapse analysis of high-rise reinforced concrete frames under long-period ground motions." *Struct. Des. Tall Special Build.* 28 (1): e1566. https://doi.org/10.1002/tal.1566.

Bai, Y., H. Wang, S. Wang, Y. Huang, Y. Chen, W. Zhang, A. Ostendorf, and X. Zhou. 2021a. "Life cycle strengthening of high-strength steels by nanosecond laser shock." *Appl. Surf. Sci.* 569 (Dec): 151118. https://doi.org/10.1016/j.apsusc.2021.151118.

Bai, Y., Y. Yue, Y. Chen, D. Luo, Y. Wang, and Y. Zhang. 2021b. "Local damage identification of high-strength circular concrete-filled steel tubes under low cycle fatigue." *Int. J. Damage Mech.* 30 (4): 559–574. https://doi.org/10.1177/1056789520963205.

Bedrinana, L. A., M. Tani, S. Kono, and M. Nishiyama. 2022. "Evaluation of the seismic performance of unbonded post-tensioned precast concrete walls with internal and external dampers. I: Experimental research." *J. Struct. Eng.* 148 (8): 04022105. https://doi.org/10.1061/(ASCE)ST.1943-541X.0003349.

Chen, Y., L. Fan, Y. Bai, J. Feng, and P. Sareh. 2020. "Assigning mountain-valley fold lines of flat-foldable origami patterns based on graph theory and mixed-integer linear programming." *Comput. Struct.* 239 (Oct): 106328. https://doi.org/10.1016/j.compstruc.2020.106328.

Chen, Y., J. Feng, and S. Yin. 2012. "Compressive behavior of reinforced concrete columns confined by multi-spiral hoops." *Comput. Concr.* 9 (5): 341–355. https://doi.org/10.12989/cac.2012.9.5.341.

Chen, Y., C. Lu, J. Yan, J. Feng, and P. Sareh. 2022. "Intelligent computational design of scalene-faceted flat-foldable tessellations." *J. Comput. Des. Eng.* 9 (5): 1765–1774. https://doi.org/10.1093/jcde/qwac082.

Chen, Y., J. Yan, and J. Feng. 2019a. "Geometric and kinematic analyses and novel characteristics of origami-inspired structures." *Symmetry* 11 (9): 1101. https://doi.org/10.3390/sym11091101.

Chen, Y., Q. Zhang, J. Feng, and Z. Zhang. 2019b. "Experimental study on shear resistance of precast RC shear walls with novel bundled connections." *J. Earthquake Tsunami* 13 (3–4): 1940002. https://doi.org/10.1142/S1793431119400025.

CS (Chinese Standard). 2010a. *Code for design of concrete structures*. GB 50010-2010. Beijing: Ministry of Housing and Urban Rural Development of the People's Republic of China.

CS (Chinese Standard). 2010b. *Code for seismic design of buildings*. GB 50011-2010. Beijing: Ministry of Housing and Urban Rural Development of the People's Republic of China.

CS (Chinese Standard). 2014. *Technical specification for precast concrete structures*. JGJ-1-2014. Beijing: Ministry of Housing and Urban-Rural Development of the People's Republic of China.

CS (Chinese Standard). 2016. *Technical standard for assembled buildings with concrete structure*. GB 51231-2016. Beijing: Ministry of Housing and Urban Rural Development of the People's Republic of China.

Dang, L. J., S. T. Liang, X. J. Zhu, R. Pang, and J. Yang. 2022. "Research on seismic behavior of unbonded post-tensioned concrete wall with vertical energy-dissipating connections." *J. Build. Eng.* 45 (Jan): 103478. https://doi.org/10.1016/j.jobe.2021.103478.

Erkmen, B. 2021. "Effects of unbonded steel layout on seismic behavior of post-tensioned precast concrete shear walls." *Bull. Earthquake Eng.* 19 (1): 179–201. https://doi.org/10.1007/s10518-020-00986-x.

Fan, W. Y., Y. Chen, J. Q. Li, Y. Sun, J. Feng, H. Hassanin, and P. Sareh. 2021. "Machine learning applied to the design and inspection of reinforced concrete bridges: Resilient methods and emerging applications." *Structures* 33 (Oct): 3954–3963. https://doi.org/10.1016/j.istruc.2021.06.110.

Govan, P., and I. Damnjanovic. 2020. "Structural network measures for risk assessment of construction projects." *ASCE-ASME J. Risk Uncertainty Eng. Syst. Part A: Civ. Eng.* 6 (1): 04019024. https://doi.org/10.1061/AJRUA6.0001041.

Gu, A. Q., Y. Zhou, Y. Xiao, Q. W. Li, and G. Qu. 2019. "Experimental study and parameter analysis on the seismic performance of self-centering hybrid reinforced concrete shear walls." *Soil Dyn. Earthquake Eng.* 116 (Jan): 409–420. https://doi.org/10.1016/j.soildyn.2018.10.003.

Guo, S. Q., and M. F. Wang. 2022. "Seismic behavior of an innovative equivalent monolithic precast shear wall under low and high axial load ratios." *Structures* 39 (May): 444–469. https://doi.org/10.1016/j.istruc.2022.03.048.

Han, R., S. Li, and W. Sun. 2022. "Effect of grouting material strength on bond strength of sleeve and acoustic emission characterization of bond failure damage process." *Constr. Build. Mater.* 324 (Mar): 126503. https://doi.org/10.1016/j.conbuildmat.2022.126503.

Henin, E., and G. Morcous. 2015. "Non-proprietary bar splice sleeve for precast concrete construction." *Eng. Struct.* 83 (Jan): 154–162. https://doi.org/10.1016/j.engstruct.2014.10.045.

Hsu, P., M. Aurisicchio, and P. Angeloudis. 2019. "Risk-averse supply chain for modular construction projects." *Autom. Constr.* 106 (Oct): 102898. https://doi.org/10.1016/j.autcon.2019.102898.

Jalali, E., H. Soltanizadeh, Y. Chen, Y. M. Xie, and P. Sareh. 2022. "Selective hinge removal strategy for architecting hierarchical auxetic metamaterials." *Nat. Commun. Mater.* 3 (1): 1–5. https://doi.org/10.1038/s43246-022-00322-7.

Jiang, Y., G. Sun, Y. He, M. Beer, and J. Zhang. 2015. "A nonlinear model of failure function for reliability analysis of RC frame columns with tension failure." *Eng. Struct.* 98 (Sep): 74–80. https://doi.org/10.1016/j.engstruct.2015.04.030.

Kang, S. M., O. J. Kim, and H. G. Park. 2013. "Cyclic loading test for emulative precast concrete walls with partially reduced rebar section." *Eng. Struct.* 56 (Nov): 1645–1657. https://doi.org/10.1016/j.engstruct.2013.07.036.

Leu, S., and C. Chang. 2015. "Bayesian-network-based fall risk evaluation of steel construction projects by fault tree transformation." *J. Civ. Eng. Manage.* 21 (3): 334–342. https://doi.org/10.3846/13923730.2014.890643.

Li, J., Y. Chen, X. Feng, J. Feng, and P. Sareh. 2021a. "Computational modeling and energy absorption behavior of thin-walled tubes with the Kresling origami pattern." *J. Int. Assoc. Shell Spatial Struct.* 62 (2): 71–81. https://doi.org/10.20898/j.iass.2021.008.

Li, J. B., Q. Q. Fan, Z. Lu, and Y. Wang. 2019. "Experimental study on seismic performance of T-shaped partly precast reinforced concrete shear wall with grouting sleeves." *Struct. Des. Tall Special Build.* 28 (13): e1632. https://doi.org/10.1002/tal.1632.

Li, W. R., H. W. Gao, R. J. Xiang, and Y. F. Du. 2021b. "Experimental study of seismic performance of precast shear wall with a new bolt-plate connection joint." *Structures* 34 (Dec): 3818–3833. https://doi.org/10.1016/j.istruc.2021.10.009.

Li, Z. D., M. C. Hu, B. Xiao, Z. Chen, V. W. Y. Tam, and Y. Y. Zhao. 2021c. "Mapping the knowledge domains of emerging advanced technologies in the management of prefabricated construction." *Sustainability* 13 (16): 8800. https://doi.org/10.3390/su13168800.

Lu, X. L., B. Y. Yang, and B. Zhao. 2018. "Shake-table testing of a self-centering precast reinforced concrete frame with shear walls." *Earthquake Eng. Eng. Vibr.* 17 (2): 221–233. https://doi.org/10.1007/s11803-018-0436-y.

Lu, Y., W. Chen, F. Xiong, H. Yan, Q. Ge, and F. Zhao. 2021. "Seismic performance of a full-scale two-story bolt-connected precast concrete composite wall panel building tested on a shake table." *J. Struct. Eng.* 147 (12): 04021209. https://doi.org/10.1061/(ASCE)ST.1943-541X.0003183.

Lu, Z., Y. Wang, J. B. Li, and Q. Q. Fan. 2019. "Experimental study on seismic performance of L-shaped partly precast reinforced concrete shear wall with cast-in-situ boundary elements." *Struct. Des. Tall Special Build.* 28 (7): e1602. https://doi.org/10.1002/tal.1602.

Mahdinia, M., M. S. Yarandi, E. Jafarinia, and A. Soltanzadeh. 2021. "Development of a new technique for safety risk assessment in construction projects based on fuzzy analytic hierarchy process." *ASCE-ASME J. Risk Uncertainty Eng. Syst. Part A: Civ. Eng.* 7 (3): 04021037. https://doi.org/10.1061/AJRUA6.0001157.

Peng, Y. Y., J. R. Qian, and Y. H. Wang. 2016. "Cyclic performance of precast concrete shear walls with a mortar-sleeve connection for longitudinal steel bars." *Mater. Struct.* 49 (6): 2455–2469. https://doi.org/10.1617/s11527-015-0660-0.

Sabatino, S., D. M. Frangopol, and Y. Dong. 2016. "Life cycle utility-informed maintenance planning based on lifetime functions: Optimum balancing of cost, failure consequences and performance benefit." *Struct. Infrastruct. Eng.* 12 (7): 830–847. https://doi.org/10.1080/15732479.2015.1064968.

Sayadi, A. A., A. B. Abd Rahman, M. Z. Bin Jumaat, U. J. Alengaram, and S. Ahmad. 2014. "The relationship between interlocking mechanism and bond strength in elastic and inelastic segment of splice sleeve." *Constr. Build. Mater.* 55 (Mar): 227–237. https://doi.org/10.1016/j.conbuildmat.2014.01.020.

Sayadi, A. A., A. B. Abd Rahman, A. Sayadi, M. Bahmani, and L. Shahryari. 2015. "Effective of elastic and inelastic zone on behavior of glass fiber reinforced polymer splice sleeve." *Constr. Build. Mater.* 80 (Apr): 38–47. https://doi.org/10.1016/j.conbuildmat.2015.01.064.

Sritharan, S., S. Aaleti, R. S. Henry, K. Y. Liu, and K. C. Tsai. 2015. "Precast concrete wall with end columns (PreWEC) for earthquake resistant design." *Earthquake Eng. Struct. Dyn.* 44 (12): 2075–2092. https://doi.org/10.1002/eqe.2576.

Sun, J., H. X. Qiu, and H. B. Jiang. 2019. "Experimental study and associated mechanism analysis of horizontal bolted connections involved in a precast concrete shear wall system." *Struct. Concr.* 20 (1): 282–295. https://doi.org/10.1002/suco.201800113.

Todut, C., D. Dan, and V. Stoian. 2014. "Theoretical and experimental study on precast reinforced concrete wall panels subjected to shear force." *Eng. Struct.* 80 (Dec): 323–338. https://doi.org/10.1016/j.engstruct.2014.09.019.

Tong, X., F. Chen, and D. Zeng. 2021. "Reliability analysis and formula adjustment for shear capacity of concrete shear walls." *Case Stud. Constr. Mater.* 14 (Jun): e00484. https://doi.org/10.1016/j.cscm.2020.e00484.

Twigden, K. M., S. Sritharan, and R. S. Henry. 2017. "Cyclic testing of unbonded post-tensioned concrete wall systems with and without supplemental damping." *Eng. Struct.* 140 (Jun): 406–420. https://doi.org/10.1016/j.engstruct.2017.02.008.

Wang, C., M. Beer, and B. M. Ayyub. 2021. "Time-dependent reliability of aging structures: Overview of assessment methods." *ASCE-ASME J. Risk Uncertainty Eng. Syst. Part A: Civ. Eng.* 7 (4): 03121003. https://doi.org/10.1061/AJRUA6.0001176.

Xia, K., X. Hu, and W. C. Xue. 2021. "Experimental studies on in-plane connections of composite beam-precast concrete shear wall under reversed cyclic loading." *Structures* 34 (Dec): 1961–1972. https://doi.org/10.1016/j.istruc.2021.08.127.

Xiao, S., Z. L. Wang, X. M. Li, K. A. Harries, Q. F. Xu, and R. D. Gao. 2021. "Study of effects of sleeve grouting defects on the seismic performance of precast concrete shear walls." *Eng. Struct.* 236 (Jun): 111833. https://doi.org/10.1016/j.engstruct.2020.111833.

Xu, G., Z. Wang, B. Wu, O. S. Bursi, X. Tan, Q. Yang, L. Wen, and H. Jiang. 2017a. "Pseudodynamic tests with substructuring of a full-scale precast box-modularized structure made of reinforced concrete shear walls." *Struct. Des. Tall Special Build.* 26 (16): e1354. https://doi.org/10.1002/tal.1354.

Xu, G. S., Z. Wang, B. Wu, O. S. Bursi, X. J. Tan, Q. B. Yang, and L. Wen. 2017b. "Seismic performance of precast shear wall with sleeves connection based on experimental and numerical studies." *Eng. Struct.* 150 (Nov): 346–358. https://doi.org/10.1016/j.engstruct.2017.06.026.

Zhang, P., W. Fan, Y. Chen, J. Feng, and P. Sareh. 2022a. "Structural symmetry recognition in planar structures using convolutional neural networks." *Eng. Struct.* 260 (Jun): 114227. https://doi.org/10.1016/j.engstruct.2022.114227.

Zhang, X., G. Zhou, S. Li, F. Zhang, and S. Zhang. 2022b. "Experimental and numerical study on seismic behavior of prestressed concrete composite shear wall." *Eng. Struct.* 266 (Sep): 114546. https://doi.org/10.1016/j.engstruct.2022.114546.